

Spectral Studies of Flaring FSRQs at GeV Energies Using Pass 8 *Fermi*-LAT Data

R. J. Britto, S. Razzaque

Department of Physics, University of Johannesburg, Auckland Park 2006, South Africa

B. Lott

Centre d'Études Nucléaires de Bordeaux-Gradignan, Université Bordeaux 1, UMR 5797/IN2P3, 33175 Gradignan, France

on behalf of the *Fermi*-LAT Collaboration

Flat spectrum radio quasars (FSRQs) are bright active galactic nuclei surrounded by gas clouds within a UV-visible intense radiation field that form the so-called broad line region (BLR). These objects emit relativistic jets from a region close to the central supermassive black hole and through the BLR. The *Fermi*-Large Area Telescope (*Fermi*-LAT) is sensitive to gamma-ray photons from ~ 30 MeV to more than 300 GeV. We have performed spectral analysis of bright FSRQs in a 5.5 year (2008-2014) data sample collected by *Fermi*-LAT, using the new Pass 8 event selection and instrument response function. Also, our study of flaring episodes in a limited time range brings interesting results while compared to the full 5.5 year data samples.

1. Modelling the BLR radiation field

FSRQs constitute a class of active galactic nuclei (AGNs) with a dense BLR in which gamma rays with energy $\gtrsim 10$ GeV are absorbed due to electron-positron pair creation, if produced deep inside the BLR. Indeed, BLR is expected to be denser in FSRQs compared to the BL Lac class.

Operating since 2008, the *Fermi* satellite has amassed more than 6 years of data, continuously surveying the whole sky [3]. The sensitivity of *Fermi*-LAT is ideal for the study of the gamma-ray absorption inside FSRQs in the 100 MeV-300 GeV range. From constraints on gamma-ray absorption we may infer limits on the location of the gamma-ray emission region in the FSRQ jets.

We expect > 10 GeV photons of FSRQs to undergo absorption in the BLR, where the target photon with energy ϵ is a UV photon from the BLR radiation field. As most of these photons are expected to come from the emission lines, we use a model that includes the 6 strongest lines (NV, Ly α , OVI Ly β , CIII NIII, NeVIII OIV, HeII Ly α) between ~ 10 to 41 eV [13].

We model these lines using a Breit-Wigner distribution, given by:

$$BW(\epsilon) = \frac{n_i \omega_i}{2 \pi [(\epsilon - \epsilon_i)^2 + (\omega_i/2)^2]}, \quad (1)$$

where n_i and ω_i are the number density and width, respectively, for a given line i .

Under the commonly used relations $L_{BLR} = 0.1 L_{disc}$ and $R_{BLR} = \sqrt{L_{disc}}$ [4, 7], where L_{BLR} is the luminosity of the BLR, R_{BLR} its radius, and L_{disc} the luminosity of the accretion disc. The photon density n_i of the radiation field for each line i can be written:

$$n_i [cm^{-3}] \simeq 1.66 \times 10^{11} \left(\frac{L_i}{10^{45} erg s^{-1}} \right) \left(\frac{10^{17} cm}{\epsilon_{i,eV} R_{BLR}^2} \right). \quad (2)$$

The opacity is derived from [5, 8] and is expressed as a function of E and z :

$$\frac{d\tau_{\gamma\gamma}(E, z)}{dx} = \frac{r_0^2}{2} \left[\frac{m^2 c^4}{E(1+z)} \right]^2 \times \sum_{i=1}^6 \left(n_i \omega_i \int_{\frac{m^2 c^4}{E(1+z)}}^{\infty} \frac{\bar{\varphi} \left[\frac{\epsilon E(1+z)}{m^2 c^4} \right] d\epsilon}{[(\epsilon - \epsilon_i)^2 + (\omega_i/2)^2] \epsilon^2} \right), \quad (3)$$

where r_0 is the classical electron radius, m the electron mass.

The $\tau_{\gamma\gamma}$ opacity in the BLR is then calculated as following:

$$\tau_{\gamma\gamma}(E, z) = a \times R_{BLR} \times \frac{d\tau_{\gamma\gamma}(E, z)}{dx}, \quad (4)$$

assuming the gamma rays are produced within $a \times R_{BLR}$, where R_{BLR} is the outer radius of BLR, and $a < 1$. Since this absorption happens at some distance from the supermassive black hole, this corrective factor that we called “ a ” represents the fraction of the BLR responsible for the absorption.

In Table I are displayed the line properties of the average spectrum of quasars we used in our model, as they were given in [13]. Since the He II Ly α line has quite large uncertainties, we arbitrary fixed its EW and relative flux to be equal to the ones of N V (uncertainty represented by (*)).

Very high energy gamma rays travelling from far distances undergo absorption in the extragalactic background light (“EBL”, mainly composed of infrared-UV radiation). This absorption is to be considered above 10 GeV and has been implemented in our studies, from the model presented in [6].

Evidence of absorption in the BLR for some FSRQs have been reported in [11, 12].

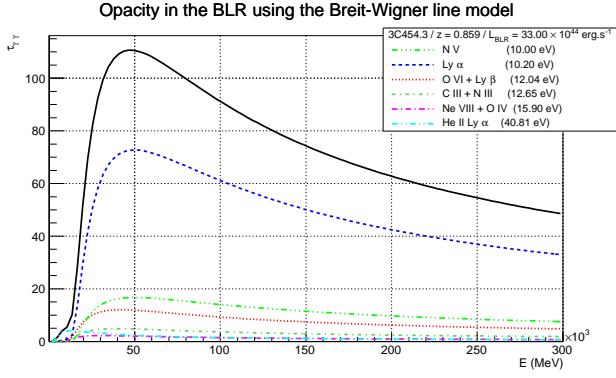


Figure 1: Opacity $\tau_{\gamma\gamma}(E, z)$ versus Energy, for 3C 454.3. The opacity sum on the 6 lines is drawn in plain black.

Table I Properties of 5 main lines of the average spectrum of quasars as compiled in [13], and He II Ly α as we defined it for this study.

Line	ϵ (eV)	EW (eV)	Relative flux
NV	10.0	0.16	0.22
Ly α	10.2	0.71	1.00
OVI Ly β	12.04	0.19	0.191
CIII NIII	12.65	0.09	0.081
NeVIII OIV	15.90	0.08	0.047
HeII Ly α	40.81	0.16*	0.22*

2. Data processing and model fitting

We have analysed data of 7 bright gamma-ray FSRQs. Plots of the spectral energy distributions (SEDs) under the label “5.5 years” have been processed from 4 August 2008 till 30 April 2014. The sources we present in this paper are listed in Table II, *LII* and *BII* being respectively the Galactic latitude and longitude in decimal degrees.

Data were processed using the Pass 8 data representation (P8_SOURCE_V4), and the Science Tools version v9-34-01. Signal is reconstructed from each source using the unbinned likelihood tool¹, applied to LAT data in the 0.1-300 GeV energy range, within a region of interest (ROI) of 10° radius. A source region extended to an additional 10° annulus accounted for all the point sources of the *Second Fermi-LAT source catalog* [9], and for the Galactic diffuse emission (template_4years_P8_V2_scaled) and the isotropic diffuse emission (isotropic_source_4years_P8V3).

We computed the SEDs for all the sources of the selected sample with the Pass 8 data representation. Additionally, for the two brightest objects of our

3C454.3 /04 Aug 2008 - 20 Jan 2014 / Pass 7 vs Pass 8

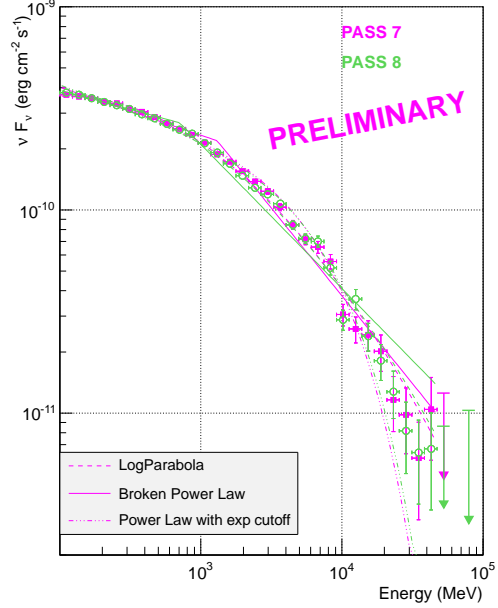


Figure 2: Comparison of the SED of 3C 454.3, produced with the Pass 7 (magenta) and Pass 8 (green) data sets.

FSRQ sample, *i.e.* 3C 454.3 and PKS 1510-089, we also computed the SEDs with the PASS 7 reprocessed dataset (P7REP_SOURCE_V15) and verified the consistency of the results with respect to the PASS 8 ones. Although some bin-to-bin fluctuations appear due to energy wise event migrations, the two SEDs (Pass 7 and Pass 8) for both the sources are compatible (as shown in Figure 2 for 3C 454.3).

A first set of fits was performed from 100 MeV till the highest energy data point (excluding upper limits), using a log-parabola (LP: $dN(E)/dE = N_0 (E/E_0)^{-\alpha-\beta \log(E/E_0)}$), with E_0 kept fixed at 297.6 MeV, and where “log” is the natural logarithm), a broken power law (BPL: $dN(E)/dE = N_0 (E/E_b)^{-\Gamma_i}$, with $i = 1$ if $E < E_b$ and $i = 2$ if $E > E_b$), and a power law with an exponential cutoff (PLEC: $dN(E)/dE = N_0 (E/E_p)^{-\Gamma_{PLEC}} \exp(-E/E_c)$, with E_p kept fixed at 412.7 MeV). Other sets of fits were performed by adding exponential factors to model the EBL absorption [6] and the opacity of the BLR.

As the fits presented in the Sections 3 and 4 are binning dependant, the values of the fit parameters vary from one choice of binning to another. Narrow data binning could held spurious fluctuations, while wide data-binning could hide features. In order to estimate this systematic effect, we do the following: a first LP fit is performed on the SED, while keeping all parameters fixed to the values obtained by the unbinned likelihood analysis, and a χ^2/ndf is returned. A second LP fit is performed with N_0 , α and β kept free,

¹ <http://fermi.gsfc.nasa.gov/ssc/data/analysis/>

Table II Characteristics of the 7 FSRQs used in this paper. Sources are ordered by decreasing flux in the 1-100 GeV energy range. Values of the luminosity in the broad line region (L_{BLR}) are taken or derived from [10, 14].

Name	RA (J2000.0)	Dec (J2000.0)	LII (deg.)	BII (deg.)	Redshift z	Flux 2FGL 1-100 GeV	Flux 1FHL 10-100 GeV	Photon index 1FGL	L_{BLR} ($10^{44} \text{ erg.s}^{-1}$)
3C 454.3	22 53 57.7	+16 08 53.1	86.11	-38.19	0.859	9.65e-8	1.35e-9	2.46619	33.00
PKS 1510-08	15 12 50.5	-09 06 00.9	351.28	40.13	0.360	4.06e-8	7.35e-10	2.40756	5.62
4C +21.35	12 24 54.5	+21 22 46.9	255.08	81.65	0.434	3.54e-8	7.43e-10	2.54717	15.80
3C 279	12 56 11.0	-05 47 20.1	305.1	57.06	0.536	2.56e-8	5.37e-10	2.32061	3.10
PKS 0454-234	04 57 03.1	-23 24 52.0	223.7	-34.9	1.003	2.27e-8	2.99e-10	2.20649	3.70
B2 1520+31	15 22 09.8	+31 44 14.3	50.16	57.02	1.484	1.76e-8	4.27e-10	2.42125	8.00
PKS (B)1424-418	14 27 56.2	-42 06 18.6	321.44	17.26	1.522	1.47e-8	2.9e-10	2.31004	8.91

E_b kept fixed to the value returned by the unbinned likelihood analysis. We compare the fits to validate that the binned fit is compatible with the unbinned fit, though results differ. These systematics could be overcome by implementing an unbinned analysis for all fitted models in future.

Our modelling study is then done by fitting the SEDs using the LP, BPL and PLEC function that all now include EBL. These fits will be reported in the Sections 3 and 4, and compared to the fits that include both EBL and BLR absorption. The latter fits are written as $LP\tau$, $BPL\tau$, and $PLEC\tau$.

The observed spectrum $F_{obs}(E)$ will then be ultimately written:

$$F_{obs}(E) = e^{-\tau_{EBL}(E,z)} e^{-a \tau_{\gamma\gamma}(E,z)} F_{int}(E), \quad (5)$$

where $F_{int}(E)$ is the LP, BPL or PLEC fitting function. Parameter a is kept free in the $[10^{-5}, 1]$ range to account for the fraction of radius of the BLR in which gamma rays may be absorbed.

The fitting procedure using the absorption models is implemented by interpolation of both the τ_{EBL} and $\tau_{\gamma\gamma}$ graphs. While comparing each “EBL + BLR absorption” fit ($LP\tau$, $BPL\tau$ or $PLEC\tau$) with the “EBL + no BLR absorption” fit (LP, BPL or PLEC), and if both fits have a $\chi^2/ndf \lesssim 1$, we obtain a p-value which indicates the discrepancy between the fit with model and the fit without model, for a given function.

3. Results on the 5.5 years of data

We present now the results on the 7 bright FSRQs during the 5.5 years period previously defined in Section 2. Data under the label “5.5 years” are processed from 4 August 2008 till 30 April 2014. In Figure 3 are presented the SEDs of 3C 454.3, PKS 1510-089, TXS 1520+31 and PKS 1424-41. Some of the fits are not visible, mainly the BPL and PLEC. The reason is that they are overwritten by the $BPL\tau$ and $PLEC\tau$ functions, for which the parameter a is very small.

We would consider having evidence for absorption in the BLR if we get all of the following:

- at least one good quality fit among one of the fits with EBL+BLR absorption ($LP\tau$, $BPL\tau$ and $PLEC\tau$);
- parameter “a” with a relatively small error bar;
- a small p-value or a bad fit of the corresponding function with only EBL absorption (LP, BPL or PLEC).

In Table III are displayed the fit parameters of the 7 sources, along with the p-values used to compare the models (with *versus* without absorption). In blue bold face are the parameters that suggest a possible BLR absorption, as some of the above conditions are partially met for 3C 454.3 (with a p-value of $6.2 \times 10^{-4} / 3.9 \sigma$ C.L.), and for TXS 1520+31 (with a p-value of $9.3 \times 10^{-3} / 2.6 \sigma$ C.L.). We have no hint of absorption for the other sources we studied.

4. Results on high state/flaring episodes

Data were analysed during flaring/high state periods for the following sources:

- 3C 454.3 (high state and giant flare) during 02 Nov-05 Dec 2010 (MJD 55502.5-55535.5)[1];
- PKS 1510-089 during 19 Feb-04 Apr 2012 (MJD 55976.0-56021.0), along with MAGIC data from the same period (MAGIC data points taken from [2]);
- PKS 1424-41 during 30 Sep 2012-27 Jul 2013 (MJD 56200.0-56500.0), as a combined series of 4 successive radio flares).

During these outburst episodes, the gamma-ray emission region can have a different location compared

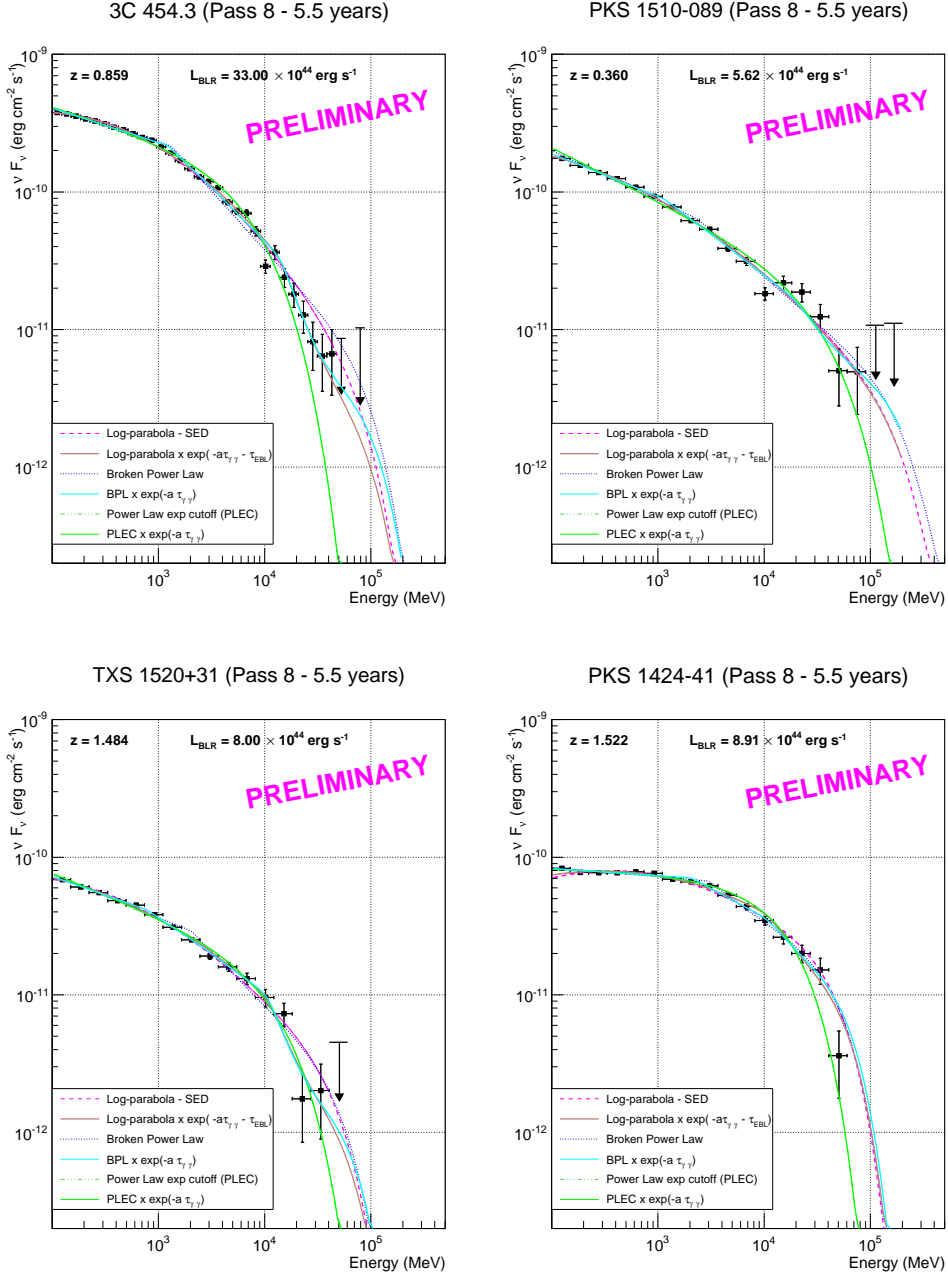


Figure 3: SEDs of 3C 454.3, PKS 1510-089, TXS 1520+31 and PKS 1424-41. *BPL* and *PLEC* fits are often hidden beneath *BPL τ* and *PLEC τ* .

to the quiescent state. In this section we present the results obtained on these three high states (Figure 4 and Table IV). Under the same criteria than the ones used in Section 3, we still find no evidence of BLR absorption, though we still have a hint of it for 3C 454.3 with a p-value of around 2.2×10^{-3} for the discrepancy between the BPL and BPL τ fits (significance of about 3σ). Due to the unusual shape of the SED of PKS 1424-41 during this series of 4 flares, all fits have a large χ^2 value.

Though we dispose of less photons in the data analysis of flaring episodes, during strong and long flares, it could be possible to constrain the location of the gamma-ray production region if it is deep enough inside the BLR.

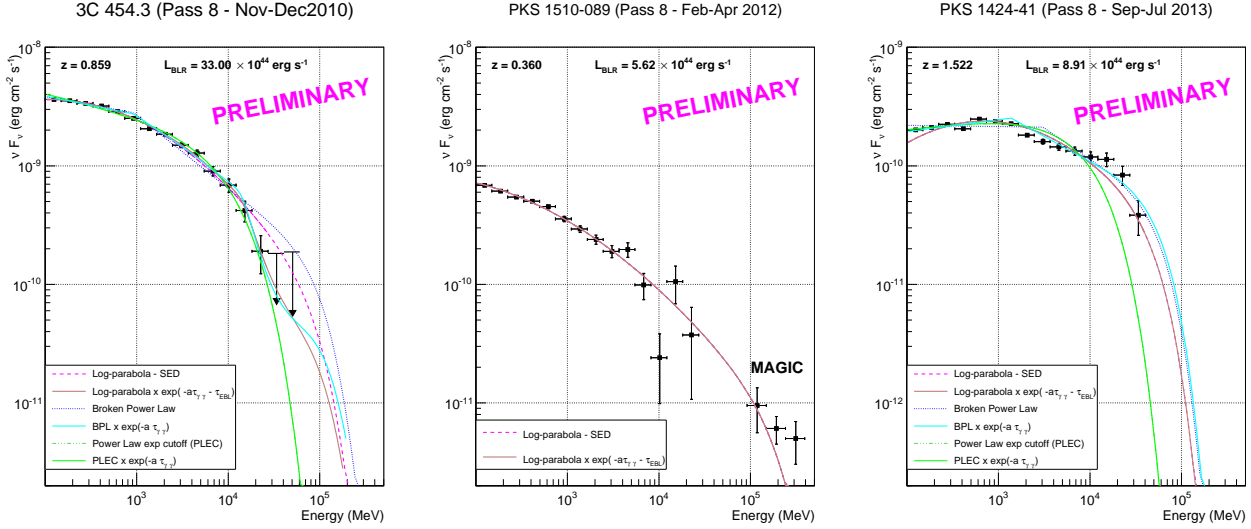


Figure 4: SEDs of 3C 454.3, PKS 1510-089 and PKS 1424-41 during the outburst periods. PLEC fits are hidden beneath PLEC τ for 3C 454.3 and PKS 1424-41. The flare of PKS 1510-089 was studied along with MAGIC data above ~ 90 GeV and the combined LAT-MAGIC SED was fitted only with LP and LP τ function (LP hidden beneath LP τ).

5. Conclusions and perspectives

We find that the gamma-gamma absorption in the BLR is not significant enough to claim discovery for the models of BLR and spectral functions we have investigated. There are hints of absorption in case of 3C 454.3 and TXS 1520+31 with significance of the order of 3σ . An implication of our results could be that the gamma-ray emission zone in FSRQs might be located outside or at the outer edge of the BLR. However, further investigation on binning effects on the SED fits are required. Future work is also expected to improve the modelling of the BLR.

Acknowledgments

The *Fermi*-LAT Collaboration acknowledges support for LAT development, operation and data analysis from NASA and DOE (United States), CEA/Irfu and IN2P3/CNRS (France), ASI and INFN (Italy), MEXT, KEK, and JAXA (Japan), and the K.A. Wallenberg Foundation, the Swedish Research Council and the National Space Board (Sweden). Science analysis support in the operations phase from INAF (Italy) and CNES (France) is also gratefully acknowledged.

Thanks to Pfsesani Van Zyl for providing the PKS 1424-41 dates during radio flares and to Julian Sitarek and the MAGIC Collaboration for providing the MAGIC data points.

References

- [1] A. A. Abdo et al, 2011, ApJL, 733:L26
- [2] J. Aleksic et al, 2014, A&A, 569, A46
- [3] W. B. Atwood et al, 2009, ApJ, 697, 1071
- [4] J. A. Baldwin & H. Netzer, 1978, ApJ, 226, 1-20
- [5] R. W. Brown, K. O. Mikaelian and R. J. Gould, 1973, ApJ L, 14, L203-L205
- [6] J. D. Finke, S. Razzaque & C. D. Dermer, 2010, ApJ, 712, 238
- [7] G. Ghisellini & F. Tavecchio, 2009, MNRAS, 397, 985
- [8] R. G. Gould & G. P. Schröder, 1967, Physical Review, 155, 5
- [9] P. L. Nolan, et al, 2012, ApJ S, 199, 31)
- [10] L. Pacciani et al, 2014, ApJ, 790, 45
- [11] J. Poutanen & B. Stern, 2010, ApJ L, 717:L118
- [12] B. Stern & J. Poutanen, 2014, ApJ, 794, 8
- [13] R. C. Telfer, W. Zheng, G. A. Kriss and A. F. Davidsen, 2002, ApJ, 565:773-785
- [14] D. R. Xiong & X. Zhang, 2014, MNRAS, 441, 4, p.3375-3395

Table III Fitting parameters and derived significances for the 7 bright FSRQs of our sample. We mention (*) when α reached the lower edge of the fitting interval.

Parameter	Model		3C 454.3	PKS 1510-089	4C +21.35	3C 279	PKS 0454-234	TXS 1520+31	PKS1424-24
function (without BLR absorption model)	LP _{unbinned}	α	2.248 \pm 0.005	2.294 \pm 0.008	2.240 \pm 0.009	2.254 \pm 0.010	2.067 \pm 0.013	2.273 \pm 0.013	2.090 \pm 0.008
	LP _{unbinned}	β	0.0897 \pm 0.0024	0.0513 \pm 0.0036	0.0445 \pm 0.0044	0.0588 \pm 0.0053	0.0793 \pm 0.0053	0.0689 \pm 0.0059	0.0753 \pm 0.0039
	PL	E_b	298 \pm 4.4	258 \pm 6.4	317 \pm 10.8	284 \pm 10.2	358 \pm 16.9	281 \pm 11.2	620 \pm 23.8
	LP	α	2.240 \pm 0.008	2.292 \pm 0.030	2.274 \pm 0.025	2.266 \pm 0.027	2.070 \pm 0.019	2.274 \pm 0.026	2.077 \pm 0.015
	LP	β	0.0980 \pm 0.0039	0.0511 \pm 0.0093	0.0404 \pm 0.0092	0.0539 \pm 0.0099	0.0761 \pm 0.0087	0.0687 \pm 0.0110	0.0713 \pm 0.0088
	BPL	Γ_1	2.242 \pm 0.345	2.363 \pm 0.030	2.280 \pm 0.028	2.332 \pm 0.029	2.138 \pm 0.016	2.317 \pm 0.033	2.066 \pm 0.010
	BPL	Γ_2	2.856 \pm 2.108	2.673 \pm 0.075	2.521 \pm 0.057	2.690 \pm 0.098	2.681 \pm 0.064	2.791 \pm 0.121	2.564 \pm 0.087
	BPL	E_b	1307 \pm 5211.8	2387 \pm 971.5	1439 \pm 573.3	2738 \pm 979.1	3062 \pm 0.3	2036 \pm 674.1	2947 \pm 573.6
	PLEC	Γ_{PLEC}	2.241 \pm 0.016	2.386 \pm 0.034	2.340 \pm 0.035	2.324 \pm 0.032	2.088 \pm 0.024	2.308 \pm 0.038	2.028 \pm 0.013
function (with BLR absorption model)	PLEC	E_c	8250 \pm 721.2	40228 \pm 13971.0	52905 \pm 28547.3	26932 \pm 8335.2	14581 \pm 2929.5	14378 \pm 3950.2	16459 \pm 2097.1
	LP τ	α	2.243 \pm 0.008	2.294 \pm 0.033	2.274 \pm 0.025	2.268 \pm 0.029	2.082 \pm 0.017	2.289 \pm 0.033	2.079 \pm 0.013
	LP τ	β	0.0876 \pm 0.0051	0.0498 \pm 0.0117	0.0404 \pm 0.0092	0.0526 \pm 0.0130	0.0590 \pm 0.0103	0.0506 \pm 0.0162	0.0542 \pm 0.0142
	BPL τ	Γ_1	2.250 \pm 0.012	2.312 \pm 0.037	2.251 \pm 0.031	2.301 \pm 0.031	2.006 \pm 0.025	2.272 \pm 0.045	2.052 \pm 0.011
	BPL τ	Γ_2	2.738 \pm 0.049	2.583 \pm 0.056	2.507 \pm 0.048	2.590 \pm 0.109	2.283 \pm 0.034	2.518 \pm 0.069	2.403 \pm 0.066
	BPL τ	E_b	1225 \pm 142.9	1152 \pm 372.0	1062 \pm 379.5	1616 \pm 743.9	544 \pm 101.1	769 \pm 315.1	2052 \pm 1.2
a	PLEC τ	Γ_{PLEC}	2.241 \pm 0.016	2.386 \pm 0.034	2.341 \pm 0.035	2.324 \pm 0.032	2.088 \pm 0.024	2.308 \pm 0.038	2.028 \pm 0.013
	PLEC τ	E_c	8251 \pm 721.4	40239 \pm 13864.7	52946 \pm 27502.4	26936 \pm 8309.2	14582 \pm 2917.7	14381 \pm 3982.3	16463 \pm 2088.6
	LP τ		0.00516 \pm 0.00185	0.00147 \pm 0.01118	0.00001 \pm 0.00139	0.00232 \pm 0.02143	0.02140 \pm 0.01007	0.01500 \pm 0.00943	0.00745 \pm 0.00515
	BPL τ		0.00666 \pm 0.00195	0.00785 \pm 0.00735	0.00001 \pm 0.00167	0.00919 \pm 0.01496	0.03641 \pm 0.00891	0.02002 \pm 0.00881	0.00558 \pm 0.00488
	PLEC τ		0.00001 \pm 0.00055	0.00001 \pm 0.00529	0.00001 \pm 0.00151	0.00001 \pm 0.00682	0.00001 \pm 0.00606	0.00001 \pm 0.01584	0.00001 \pm 0.00248
χ^2 (ndf) without abs. model	LP _{unbinned}		36.419 (30)	7.454 (17)	18.821 (16)	5.288 (16)	14.783 (16)	8.988 (15)	36.173 (16)
	LP		29.316 (27)	7.278 (14)	13.009 (13)	4.609 (13)	11.516 (13)	6.448 (12)	22.826 (13)
	BPL		45.647 (26)	9.963 (13)	11.269 (12)	7.290 (12)	28.960 (12)	8.826 (11)	19.366 (12)
	PLEC		42.999 (26)	13.115 (13)	21.817 (12)	7.422 (12)	17.094 (12)	5.158 (11)	17.037 (12)
χ^2 (ndf) with abs. model	LP τ		17.591 (26)	7.245 (13)	13.017 (12)	4.582 (12)	6.526 (12)	3.181 (11)	20.495 (12)
	BPL τ		25.071 (25)	7.242 (12)	9.870 (11)	5.694 (11)	4.282 (11)	2.069 (10)	17.474 (11)
	PLEC τ		43.017 (26)	13.117 (13)	21.823 (12)	7.424 (12)	17.095 (12)	5.159 (11)	17.042 (12)
$\Delta\chi^2$ (ndf)	LP/PL τ		1.173e+01	3.360e-02	7.208e-03	2.747e-02	4.989e+00	3.267e+00	2.331e+00
	BPL/BPL τ		2.058e+01	2.720e+00	1.399e+00	1.596e+00	2.468e+01	6.757e+00	1.892e+00
	PLEC/PLEC τ		1.812e-02	1.888e-03	6.614e-03	1.464e-03	1.646e-03	6.277e-04	4.025e-03
p-value	LP/LP τ		6.166e-04	8.546e-01	9.323e-01	8.684e-01	2.551e-02	7.070e-02	-
	BPL/BPL τ		-	9.908e-02	2.369e-01	2.064e-01	-	9.337e-03	-
	PLEC/PLEC τ		-	-	-	-	-	-	-

Table IV Fitting parameters and derived significances for the 3 flares we studied in our FSRQ sample. We mention (*) when a reached the lower edge of the fitting interval.

Parameter	Model	3C 454.3 (Nov-Dec 2010)	PKS 1510-089 (Feb-Apr 2012)	PKS1424-24 (Sep 2012-Jul 2013)
function (without BLR absorption model)	LP_unbinned α	2.152 ± 0.008	2.268 ± 0.027	2.022 ± 0.010
	LP_unbinned β	0.0895 ± 0.0036	0.0451 ± 0.0108	0.0766 ± 0.0052
	PL E_b	286 ± 8.9	260 ± 6.0	940 ± 35.4
	LP α	2.153 ± 0.016	2.299 ± 0.040	2.069 ± 0.014
	LP β	0.0879 ± 0.0088	0.0569 ± 0.0117	0.1134 ± 0.0120
	BPL Γ_1	2.140 ± 0.022	2.367 ± 0.038	2.010 ± 0.003
	BPL Γ_2	2.617 ± 0.036	2.867 ± 0.076	2.530 ± 0.055
	BPL E_b	921 ± 0.4	2603 ± 912.7	3062 ± 1.6
	PLEC Γ_{PLEC}	2.183 ± 0.034	2.269 ± 0.049	1.903 ± 0.021
	PLEC E_c	9981 ± 2111.4	7921 ± 2586.5	8361 ± 1117.7
function (with BLR absorption model)	LP τ α	2.157 ± 0.018	2.299 ± 0.022	2.069 ± 0.014
	LP τ β	0.0764 ± 0.0116	0.0569 ± 0.0065	0.1134 ± 0.0120
	BPL τ Γ_1	2.156 ± 0.029	-	1.900 ± 0.019
	BPL τ Γ_2	2.518 ± 0.050	-	2.426 ± 0.036
	BPL τ E_b	921 ± 0.2	-	1375 ± 0.2
	PLEC τ Γ_{PLEC}	2.183 ± 0.034	-	1.903 ± 0.021
	PLEC τ E_c	9983 ± 2113.2	-	8361 ± 1135.7
a	LP τ	0.00703 ± 0.00551	0.04667 ± 0.04550	0.00001 ± 0.00132
	BPL τ	0.01059 ± 0.00591	-	0.00001 ± 0.00320
	PLEC τ	0.00001 ± 0.00629	-	0.00001 ± 0.00108
$\chi^2(ndf)$ without abs. model	LP_unbinned	4.553 (14)	67.828 (17)	79.634 (15)
	LP	4.041 (11)	20.807 (14)	37.481 (12)
	BPL	13.158 (10)	15.137 (13)	101.358 (11)
	PLEC	6.912 (10)	37.461 (13)	77.643 (11)
$\chi^2(ndf)$ with abs. model	LP τ	0.928 (10)	20.807 (13)	37.489 (11)
	BPL τ	3.780 (9)	-	24.648 (10)
	PLEC τ	6.914 (10)	-	77.652 (11)
$\Delta\chi^2$ (ndf)	LP/PL τ	3.113e+00	6.395e-11	7.583e-03
	BPL/BPL τ	9.378e+00	-	7.671e+01
	PLEC/PLEC τ	1.586e-03	-	9.270e-03
p-value	LP/PL τ	7.769e-02	-	-
	BPL/BPL τ	2.195e-03	-	-
	PLEC/PLEC τ	0.000e+00	-	-

